6th International Conference on Advances in Experimental Structural Engineering
11th International Workshop on Advanced Smart Materials and Smart Structures Technology
August 1-2, 2015, University of Illinois, Urbana-Champaign, United States

# Multi-Scale Structural Health Monitoring Technologies

**Y.L. Xu [1] and B.F. Spencer [2]**

1 *Chair Professor, Department of Civil and Environmental Engineering, The Hong Kong Polytechnic University, Kowloon, Hong Kong.*
*E-mail: ceylxu@polyu.edu.hk.*
2 *Nathan M. New Mark Professor, Department of Civil and Environmental Engineering, University of Illinois at Urbana-Champaign, Illinois, USA.*
*E-mail: bfs@uiuc.edu.*

**ABSTRACT**

This study presents multi-scale structural health monitoring (SHM) technologies for large civil structures. It involves four major tasks: (1) the multi-scale finite element modeling of a large civil structure that can integrate the global structural model equipped with global sensors with the local structural details installed with local sensors; (2) the development of multi-scale model updating method that uses multi-scale updating parameters and objective functions together with the Kriging method; (3) the optimal placement of multi-type sensors that can integrate global and local sensors, minimize the required number of sensors, and increase the accuracy of damage detection via best response reconstruction; and (4) the development of multi-scale damage detection method that can synthesize the measurement data from different sensors with different scales. The accuracy of the proposed technologies is validated by conducting various experimental studies.

**KEYWORDS:** *Multi-scale, structural health monitoring, large civil structures, damage detection*

## 1. INTRODUCTION

Many innovative civil structures have been constructed around the world. These structures are subject to harsh environments, which present many challenges to professionals for the functionality, safety and sustainability of the structures. The structural health monitoring (SHM) technologies have been regarded as a cutting-edge approach to providing a better solution for the problems. Over the past two decades, significant effort has been dedicated to vibration-based methods for damage detection in terms of measured global structural responses. However, most large civil structures are complex structures, comprising tens of thousands of structural components of different sizes and connected to one another in different ways. Local damage often does not significantly affect the global responses of a structure, making global response-based damage analysis inaccurate and sometimes impossible. Moreover, the number of sensors in an SHM system for a large civil structure is always limited, and the sensors may not directly monitor the locations of structural defects. Therefore, the successful application of damage detection methods to a large civil structure is very limited.

This study presents multi-scale structural health monitoring (SHM) technologies for large civil structures. It involves four major tasks: (1) the multi-scale finite element modeling of a large civil structure; (2) the development of multi-scale model updating method; (3) the optimal placement of multi-type sensors; and (4) the development of multi-scale damage detection method. The accuracy of the proposed technologies is validated by conducting various experimental studies.

## 2. MULTI-SCALE FINITE ELEMENT MODELING

In practice, a large civil structure is often modeled via finite element (FE) method using a combination of beam, shell, solid, and other elements of similar scale for the static and dynamic analyses at a global level. Stress concentration, crack initiation and propagation, fatigue, and fracture are local phenomena that are often not represented in the global structural model. However, many types of defects are locally generated at the material points and sectional levels and may evolve into a global structural damage and possibly cause structural failure. Thus, a multi-scale FE modeling of large civil structures has recently attracted increasing attention in the field of structural health monitoring [1]. Multi-scale modeling of a large civil structure mainly aims to simulate and evaluate simultaneously its structural performance at both the macro- and micro-scales. This section first

presents a new mixed-dimensional FE coupling method that can achieve both displacement compatibility and stress equilibrium at the interface between the different element types. The new mixed-dimensional FE coupling method is then used to establish the multi-scale FE model of a transmission tower.

## 2.1. Interface Coupling of Mixed-Dimensional Elements

Taking the interface coupling of beam-to-solid elements as an example, the displacement constraint can be established in the sense that the displacement of beam at the interface equals to the generalized displacement of solid at the interface, which can be expressed as

$$\boldsymbol{c}(\boldsymbol{u}_B, \boldsymbol{u}_S) = \boldsymbol{u}_B - \boldsymbol{C}\boldsymbol{u}_S = 0 \tag{2.1}$$

where $\boldsymbol{u}_B$ and $\boldsymbol{u}_S$ are the nodal displacement vector of beam and solid, respectively, at the interface; $\boldsymbol{C}$ is the coefficient matrix of the displacement constraint equation. The term of $\boldsymbol{C}\boldsymbol{u}_S$ can be seen as the generalized displacements of the solid, matching with the beam displacements $\boldsymbol{u}_B$ at the interface and obtained by weighting the coefficient matrix $\boldsymbol{C}$ over the solid displacement vector $\boldsymbol{u}_S$ at the interface. In consideration that the sum of virtual work done by the corresponding forces at the interface of the two types of elements shall be zero, the constraint equation of nodal forces at the interface can be expressed as

$$\boldsymbol{F}_S = -\boldsymbol{C}^{\mathrm{T}}\boldsymbol{F}_B \tag{2.2}$$

where $\mathbf{F}_B$ and $\mathbf{F}_S$ are the nodal force vector of beam and solid, respectively. It is interesting to see that the coefficient matrix $\boldsymbol{C}^{\mathrm{T}}$ of the force constraint equation is the transpose of the coefficient matrix $\boldsymbol{C}^{\mathrm{T}}$ of the displacement constraint equation. The coefficient matrix of the force constraint equation can be regarded as a distribution matrix to distribute the forces or moment at the node of the beam to the nodes of the solid at the interface. The satisfaction of both Eq. (2.1) and Eq. (2.2) can achieve both displacement compatibility and stress equilibrium between the different element types. Furthermore, Eq. (2.2) indicates that the distribution coefficients in the force distribution matrix are the corresponding nodal forces of the solid at the interface under unit force or moment. Hence, the coefficient matrix of the force constraint equation actually refers to the nodal forces along the cross-section of the solid under unit force or moment. Based on this principle, a new numerical method compatible with commercial FE codes has been developed to figure out the coefficient matrix of the force constraint equation. Once it is obtained, the coefficient matrix of the displacement constraint equation can be easily found, and both displacement compatibility and stress equilibrium conditions at the interface are satisfied.

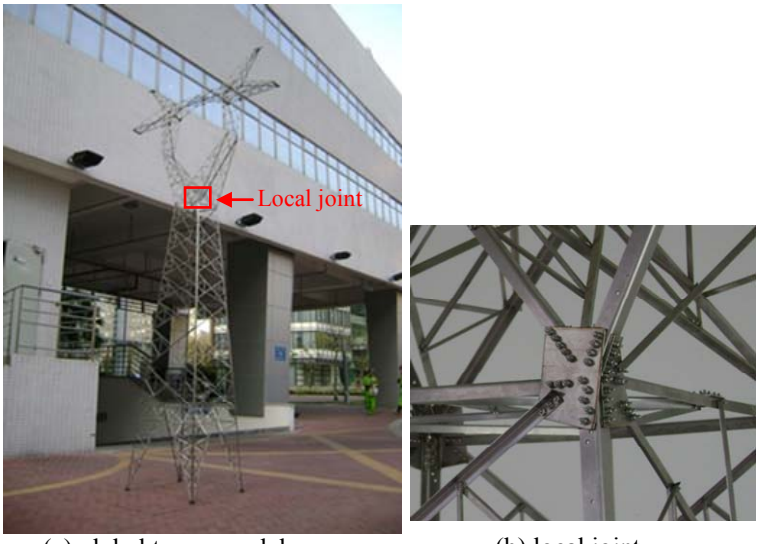


(a) global tower model (b) local joint

Figure 2.1 Physical model of a transmission tower

## 2.2. A Physical Model of a Transmission Tower

In order to verify the accuracy of multi-scale modeling and analysis, a physical model of a transmission tower structure was built (see Figure 2.1). The tower is assembled from 23 types of angle members, which are

connected to each other at joint plates with bolts. The angle members and gusset plates were tailor-made in a factory by using the stainless steel plates. The completed tower model had 930 angle members, 402 gusset plates and 3649 bolts. The static tests were carried out on the physical model of the transmission tower to obtain the strain and displacement responses of the tower under a concentrated load. The hammer tests were carried out on the physical model of the transmission tower to identify the natural frequencies and modal shapes of the tower. The test data will be then used for validating the multi-scale modeling and analysis results.

## 2.3. Multi-Scale Modeling of the Transmission Tower

For a transmission tower, there are many complex problems to deal with in the process of multi-scale modeling, such as the interface coupling of mix-dimensional elements and the contact problem between bolts and plates. It is therefore more convenient to build the multi-scale model of the transmission tower using commercial FE software. The FE software ANSYS is used in this study together with the self-written supplemental programs for multi-scale modeling and analysis of the transmission tower structure.

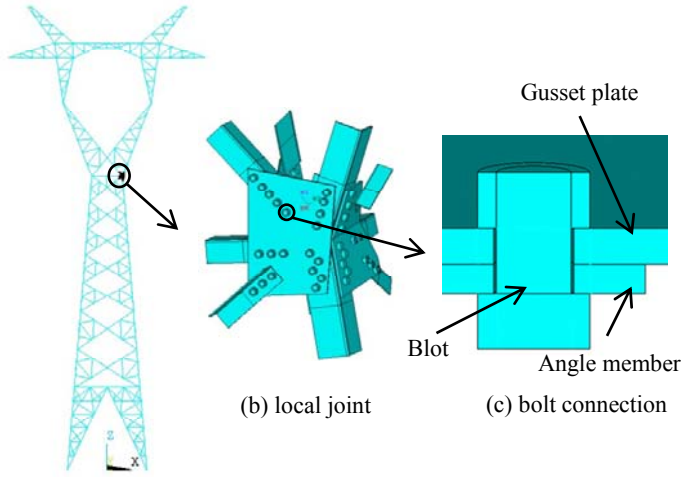


Figure 2.2 Multi-scale model of a transmission tower

For the sake of a clear demonstration, only one typical and most important tower joint between the crank arm and the tower body is selected to construct a detailed local FE joint model (see Figure 2.2b). The selected joint consists of 9 angle members of a shortened length, 3 gusset plates and 40 bolts. In order to accurately simulate the bolt connection, all the components of the joint are modeled using solid elements. Consequently, the 20-node SOLID95 elements of higher order, which can simulate irregular shapes with no loss in accuracy, are used to model angle members, gusset plate and bolts of the selected joint. Apart from this joint, all other members of the tower are modeled using beam elements and all other joints are modeled as rigid joints. The completed multi-scale model of the transmission tower is shown in Figure 2.2a together with the local joint model and the bolt connection shown in Figure 2.2b and Figure 2.2c respectively. It is noted that there is an interface for each of 9 angle members used in the joint between the global tower model and the local joint model. The interface of the angle member between the solid and beam elements is coupled by using the proposed interface coupling method. Another complex problem in the local modeling of the joint is the interaction between different components for bolt connection, such as the contact between the bolt and the angle member, the contact between the bolt and the gusset plate, and the contact between the angle member and the gusset plate. These interactions are achieved by using the contact elements TARGE170 and CONTA174 of surface-to-surface type, which avoid one element to penetrate into another. Furthermore, these contact elements can simulate friction forces between the two surfaces according to the Mohr–Coulomb law.

## 3. MULTI-SCALE MODEL UPDATING

Although there is less uncertainty in the multi-scale model than in the conventional FE model, multi-scale model updating shall be performed to ensure the quality of the multi-scale model of the transmission tower at both macro and micro levels. A multi-scale model updating method using the multi-objective optimization and Kriging method is therefore presented in this section.

### 3.1. Parameters and Objective Functions of Multi-Scale Model Updating

In FE model updating, a set of key parameters of the structure is updated by means of minimizing the objectives formed by the residuals between the experimental and FE analytical results of dynamic characteristics and/or responses. Compared with conventional FE model updating, the multi-scale model updating requires the updating of both global and local models simultaneously. Thus, the updating parameters are selected from both global and local models. In this study, the global parameters of the structure refer to the elastic moduli of angle members, the densities of angle members, and the lumped masses at the rigid joints. The local parameters refer to the elastic moduli of gusset plates and bolts and the densities of gusset plates and bolts of the selected local joint. Accordingly, the structural responses used to calculate the residuals are classified as either global responses or local responses. In this study, the dynamic characteristics and the static responses of displacement and strain from the global model are regarded as global characteristics or global responses while the strain responses of the selected local joint are taken as local responses.

Multi-objective optimization algorithm is developed to deal with the minimization of a vector of objective functions subject to a number of constraints or bounds. A multi-objective optimization problem (MOP) is formulated as follows:

$$\begin{aligned} &\text{minimize} \quad J(\theta) = \{J_1(\theta), J_2(\theta), ..., J_q(\theta)\} \\ &\text{subject to} \quad \theta_l \le \theta \le \theta_u \end{aligned} \tag{3.1}$$

where θ is the vector of updating parameters; $\theta_l$ and $\theta_u$ are the lower and upper bounds of $\theta$; and J($\theta$) is a vector of objective functions. It should be noted that the optimality of MOP is not obvious because a solution $\theta$ that simultaneously minimizes all sub-objectives does not generally exist. Instead, the Pareto optimality is used to characterize the objectives. The Pareto optimality is a solution in which it is impossible to make any one objective better off without making at least one objective worse off. Here, the preferred FE model is selected by using the residual of each Pareto optimal solution. The solution with the minimum residual is selected as the preferred FE model with the updated parameters. In this study, non-dominated sorting genetic algorithm-II (NSGA-II) is employed for the implementation of multi-objective optimization to find the Pareto optimal solution. In the algorithm NSGA-II, the objective functions are calculated for every iteration process. Therefore, the multi-scale analysis of the structure is required to be carried out for each iteration process, which needs huge computation time. To reduce the computation effort of the model updating, the Kriging meta-model is built and used to replace the multi-scale analysis in the iterative optimization process. In the Kriging meta-model, the unknown functions are the residuals of displacements, strains, natural frequencies and MAC. The variables are updating parameters, such as elastic modulus and density.

### 3.2. Multi-Scale Model Updating of the Transmission Tower

Based on the test types and results of the transmission tower, the multi-objective optimization model is established for multi-scale model updating, which consists of objective functions, constraints and updating parameters. Firstly, the 31 residuals of displacements, strains, natural frequencies and MACs are calculated. The 3 objective functions are defined by these residuals as follows:

$$\begin{aligned} J_1(\theta) &= \sum_{i=1}^{9} \left| R_i^{frequency} \right| + \sum_{i=1}^{9} \left| R_i^{MAC} \right| \\ J_2(\theta) &= \sum_{i=1}^{3} \left| R_i^{displacement} \right| + \sum_{i=1}^{6} \left| R_i^{strain} \right| \\ J_3(\theta) &= \sum_{i=7}^{10} \left| R_i^{strain} \right| \end{aligned} \tag{3.2}$$

where $J_1(\boldsymbol{x})$ and $J_2(\boldsymbol{x})$ are the global objective functions; and $J_3(\boldsymbol{x})$ is the local objective function. The selection of effective updating parameters is a crucial step in model updating. It is impractical to associate one updating parameter with each element. Here, one model parameter is used for all the angle members with the same thickness. The sensitivities are then used for the selection of parameters, in which parameters with lower sensitivity are eliminated. As a result, a total of 13 updating parameters are selected. The selected updating parameters refer to 7 elastic moduli, 4 densities and 2 lumped masses.

The updating results show that the maximum change in all the updating parameters is 16% of the equivalent modulus of elasticity of the gusset plates. This is because the strain responses of the gusset plates predicted by the initial model have the largest error compared with the test results. Furthermore, there is only one updating parameter with a change more than 10% among the seven updating parameters of elastic modulus, but there are four updating parameters with a change more than 10% among the six updating parameters of mass (including

densities and lumped masses). This is because the masses of the gusset plates and bolts are about 15.6% of the total mass of the transmission tower but it is difficult to accurately estimate the masses of the gusset plates and bolts. Both the initial and updated multi-scale FE models of the transmission tower are used to calculate the strain and displacement responses of the tower under the concentrated load. The results from the initial and updated multi-scale model are then compared with those from the static tests. The comparison results of the displacement responses show that the results obtained from the updated multi-scale model are closer to the test results compared with those from the initial model. The comparison results of strain responses manifest that the strain responses of the main angle members of the local joint calculated from the updated multi-scale model are more accurate than those from the initial model. The maximum errors of strains from the initial and updated multi-scale models are 30.37% and 9.77%, respectively, compared with the test results. The modal analysis is also carried out using the initial and updated multi-scale models of the transmission tower. The natural frequencies are obtained and compared with the test results. The maximum errors using the updated multi-scale model occurs at the sixth natural frequency with a relative error of 5.41%. The maximum error of the frequencies of the initial model is 6.98% for the third mode of vibration.

## 4. MULTI-TYPE SENSOR PLACEMENT

This section investigates a practical and challenging problem on how to place multi-type sensors with the aim of best reconstruction of multi-scale responses at key locations. Given that strain measurement sensors are usually used to record local responses, whereas displacement and acceleration responses are applied to obtain global responses such as natural frequencies and mode shapes, the three types of sensors commonly used in SHM, namely, accelerometers, strain gauges and displacement sensors, are considered. The locations of the multi-type sensor system are optimized simultaneously, and the measurements from the three types of sensors are integrated to reconstruct the structural responses of the structure at key locations with the Kalman filter algorithm. The posteriori error covariance is selected as a performance measure of reconstruction accuracy in the optimization [**Error! Reference source not found.**]. A simply-supported overhanging steel beam is analyzed as a case study.

### 4.1. Framework

The modally reduced order model of a structure with a proportional damping can be described by the following time-invariant continuous state space equation in modal coordinate as

$$\begin{cases} \dot{\mathbf{x}}(t) = \mathbf{A}_c\mathbf{x}(t) + \mathbf{B}_c\mathbf{u}(t) \\ \mathbf{y}(t) = \mathbf{C}_c\mathbf{x}(t) + \mathbf{D}_c\mathbf{u}(t) \end{cases} \tag{4.1}$$

By including the modeling error and measurement noise, the continuous-time state space model in Eq. (4.1) can be transferred into a discrete-time state space model as

$$\begin{aligned} \mathbf{x}_{k+1} &= \mathbf{A}_d\mathbf{x}_k + \mathbf{B}_d\mathbf{u}_k + \mathbf{w}_k \\ \mathbf{y}_k &= \mathbf{C}_d\mathbf{x}_k + \mathbf{D}_d\mathbf{u}_k + \mathbf{v}_k \end{aligned} \tag{4.2}$$

where $\mathbf{x}_k = \mathbf{x}(k\Delta t) \in \Re^{2r}$ is the discrete-time state vector with $\Delta t$ being the sampling interval; $\mathbf{w}_k \sim N(0, \mathbf{Q})$ and $\mathbf{v}_k \sim N(0, \mathbf{R})$ represent the independent, white Gaussian modeling error and measurement noise vectors, respectively. The Kalman filter gives an unbiased and recursive algorithm to optimally estimate the unknown state vector of a linear dynamic system [3] as:

$$\hat{\mathbf{x}}_{k+1} = \left(\mathbf{A}_d - \mathbf{K}_k\mathbf{C}_d^m\right)\hat{\mathbf{x}}_k + \left(\mathbf{B}_d - \mathbf{K}_k\mathbf{D}_d^m\right)\mathbf{u}_k + \mathbf{G}_k\left(\mathbf{y}_{k+1}^m - \mathbf{D}_d\mathbf{u}_{k+1}\right) \tag{4.3}$$

in which $\mathbf{y}^m$ denotes the sensor measurements; $\mathbf{C}_d^m$ and $\mathbf{D}_d^m$ are composed of the mode shapes with measured DOFs; and $\mathbf{G}_k$ is the Kalman gain. The reconstructed responses at the key locations are then

$$\mathbf{y}_k^e = \mathbf{C}_d^e\hat{\mathbf{x}}_k + \mathbf{D}_d^e\mathbf{u}_k \tag{4.4}$$

$\mathbf{C}_d^e$ and $\mathbf{D}_d^e$ are composed of modal shapes corresponding to DOFs of the key location, where no sensors are installed. The accuracy of the reconstructed responses can be measured by the reconstruction error $\boldsymbol{\delta}_k$ as

$$\boldsymbol{\delta}_k = \left(\mathbf{C}_d^e\hat{\mathbf{x}}_k + \mathbf{D}_d^e\mathbf{u}_k\right) - \left(\mathbf{C}_d^e\mathbf{x}_k + \mathbf{D}_d^e\mathbf{u}_k\right) = \mathbf{C}_d^e\left(\hat{\mathbf{x}}_k - \mathbf{x}_k\right) \tag{4.5}$$

The response reconstruction error covariance matrix is

$$\mathbf{\Delta}_k = E\left[\boldsymbol{\delta}_k \boldsymbol{\delta}_k^T\right] = \mathbf{C}_d^e \mathbf{P}_k^x \left(\mathbf{C}_d^e\right)^T \tag{4.6}$$

where $\mathbf{P}_k^x$ is the posteriori state error covariance of state vector at a time step. The number and location of sensors are optimally designed by selecting the proper output matrix $\mathbf{C}_d^m$ and transmission matrix $\mathbf{D}_d^m$ to minimize the trace of stable reconstruction error covariance matrix. Notably, the output influence matrix $\mathbf{C}_d^e$ or $\mathbf{C}_d^m$ tends to be highly ill-conditioned because the strain, the displacement and the acceleration have significantly different orders of magnitude. Thus, the reconstruction errors are normalized as

$$\tilde{\boldsymbol{\delta}}_k = \left(\mathbf{R}^e\right)^{-1/2} \boldsymbol{\delta}_k = \left(\mathbf{R}^e\right)^{-1/2} \mathbf{C}_d^e \left(\hat{\mathbf{x}}_k - \mathbf{x}_k\right) = \tilde{\mathbf{C}}_d^e \left(\hat{\mathbf{x}}_k - \mathbf{x}_k\right) \tag{4.7}$$

where $\mathbf{R}^e$ is covariance matrix of different type measurement noise. The objective and constraint functions of the sensor location selection can be expressed as

$$\min\left\{\tilde{\sigma}_{avg}^2\right\} = \min\left\{trace(\tilde{\mathbf{C}}_d^e \overline{\mathbf{P}} \tilde{\mathbf{C}}_d^{eT})/N\right\} \tag{4.8}$$

## 4.2. Case Study

A simply-supported overhanging steel beam is modeled as a two-dimensional Euler-Bernoulli beam, constrained by a hinge support and a roller support (see Figure 4.1). The model consists of 40 elements and 41 nodes with a total of 123 DOFs. The effect of the exciter on the beam is modeled by a mass element and a spring element in the FE model. The first seven frequencies are 6.03, 8.42, 17.73, 41.60, 64.42, 71.75, and 101.14 Hz.

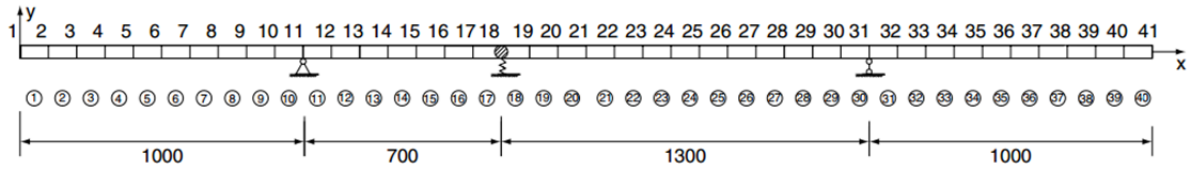


Figure 4.1 FE model of simply-supported overhanging beam (unit: mm)

All the element strains, nodal vertical displacements, and accelerations, except for the locations at supports, are considered as the key responses to be reconstructed. They are also regarded as initial candidate locations for sensors. Thus, totally 118 sensor locations are selected as the initial candidates, including 40 for strain gauges, 39 for displacement transducers, and 39 for accelerometers. The strain gauges are assumed to be attached on the upper face at the center of each element; displacement transducers and accelerometers are installed vertically on the structure. A random force with frequency ranging from 0.5 Hz to 100 Hz is applied to node 18 to generate structural vibration. The first seven modes are selected to determine the number and optimal locations of the multi-type sensors and reconstruct the multi-scale responses with the proposed method. The standard deviations of the measurement noise for the strain gauge, displacement transducer, and accelerometer are assumed as 0.201, 0.01 mm, and 0.189 m/s2, respectively.

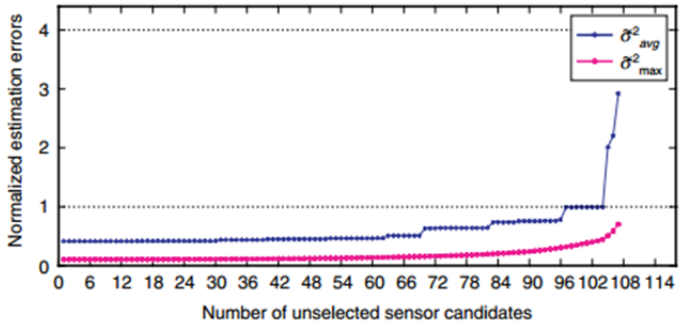


Figure 4.2 Variation of reconstruction errors with number of sensors

Figure 4.2 shows variation of reconstruction errors with number of sensors. With the decrease in the sensor number, the errors increase. By selecting an allowable response reconstruction error, the type, number and optimal location of the sensors can be determined. In this case study, 11 sensor locations are selected, including five locations for strain gauges, two for displacement transducers, and four for accelerometers, as shown in Figure 4.3.


Figure 4.3 Sensor locations on the simply-supported overhanging beam

Further studies clearly indicate that the heterogeneous fusion of data from multi-type sensors provides a more detailed and accurate reconstruction of multi-scale structural responses, which can provide comprehensive information for SHM of large civil structures with limited number of sensors. The experimental work carried out on the same beam also confirms the theoretical results [2].

## 5. MULTI-SCALE DAMAGE DETECTION

This section provides a multi-scale damage detection method in conjunction with response reconstruction. Radial-basis-function (RBF) network is adopted to estimate the strain and displacement mode shapes of the structure at the unmeasured locations based on the information measured by the sensors. The natural frequencies and mode shapes given by the RBF network are then used for the response reconstruction. The differences in the reconstructed responses between the undamaged and damaged structure are finally used to identify the damage location and extent. A simply-supported overhanging steel beam is analyzed to demonstrate the superiority of the proposed damage detection method.

### 5.1. RBF Network for Response Reconstruction of Damaged Structure

It can be proved that RBF network is capable of providing arbitrarily good approximation to any prescribed function using only a finite number of parameters [4]. The output of the network is a function of the input vector and it is given by

$$f_j(\mathbf{x}) = \sum_{i=1}^{N} w_i \psi\left(\left\|\mathbf{x} - c_i\right\|\right) \tag{5.1}$$

where $N$ is the number of neurons in the hidden layer; $c_i$ is the center vector for neuron $i$; $w_i$ is the weight of neuron $i$ in the linear output neuron; and $\psi$ is named as the radial basis function that depends only on the distance from a center vector and it is radially symmetric about that vector. The input of the network is the frequencies and mode shapes of the damaged structure at the sensor locations, which can be extracted by experimental model analysis (EMA) from the measured data. These data are then used to train the BRF network to estimate the strain and displacement mode shapes of the structure at the unmeasured locations. The response reconstruction method presented in Section 4 is finally used to estimate the responses of the structure at the unmeasured locations. The flow chart of response reconstruction of the damaged structure is shown in Fig. 5.1.

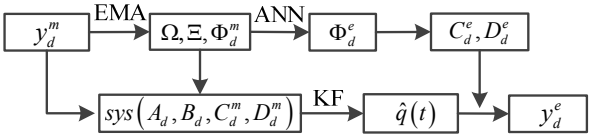


Figure 5.1 Flow chart of response reconstruction of damaged structure

### 5.2. Response Sensitivity-Based FE Model Updating and Damage Detection

Since dynamic response is a nonlinear function of damage parameter $\boldsymbol{\theta}$, an iterative procedure using a gradient-based optimization can be employed to obtain the damage parameter as

$$\mathbf{S}^k \Delta\boldsymbol{\theta}^{k+1} = \Delta\mathbf{Y}^k \tag{5.2}$$

where $\mathbf{S}^k = \mathbf{S}\left(\boldsymbol{\theta}^k\right) = \partial\mathbf{Y}\left(\boldsymbol{\theta}^k\right)/\partial\boldsymbol{\theta}$ is the sensitivity matrix for the k-th iteration with $\mathbf{S}_{ij}^k = \partial\mathbf{Y}_i\left(\boldsymbol{\theta}^k\right)/\partial\boldsymbol{\theta}_j$; $\Delta\mathbf{Y}^k = \mathbf{Y}_d - \mathbf{Y}_a\left(\boldsymbol{\theta}^k\right)$ is the response residuals between the damaged and undamaged structure; and $\boldsymbol{\theta}^k = \sum_{l=1}^{k} \Delta\boldsymbol{\theta}^l$ is the cumulative damage parameter in all the k-th iterations. $\mathbf{S}^k$ and $\Delta\mathbf{Y}^k$ are assembled by stacking the columns of sensitivity sequences and response discrepancy sequences, respectively. A strategy of sparse regularization is used to find the solution of Eq.(5.2) since damage usually occurs at very few components or locations of a structure.

## 5.3. Case Study

The simply-supported overhanging steel beam discussed in the last section is used as a case study. A broadband stochastic force with a frequency bandwidth ranging from 2 Hz to 82 Hz and a standard deviation of 30 N is applied on node 18 vertically. The first two modal damping ratios are set as $\xi_1 = \xi_2 = 0.01$. Time step is 1/500s and sample duration is 12s. Noise corruption is simulated by adding normally distributed random noise to the noise-free response. The noise amplitude is set as $0.201\,\mu\varepsilon$, $0.01\,\text{mm}$ and $0.04\ \text{m}/\text{s}^2$ for strain, displacement and acceleration, respectively, according to the laboratory measurement data. The signal-noise-ratio (SNR) is approximately 2%~3% .

The damage is simulated as the reduction of elastic modulus of the element. A case of 12% reduction of elastic modulus of element 7 and 23% reduction of element 23 is employed here to represent a multi-damage scenario to investigate the effectiveness of the proposed multi-scale damage detection method with and without response reconstruction. Damage can be modeled as $\mathbf{K}^d = \mathbf{K}^u + \sum_{i=1}^{Ne} \theta_i \mathbf{K}_i \left(-1 \le \theta_i \le 0\right)$ while inertial properties are assumed unchanged before and after damage.

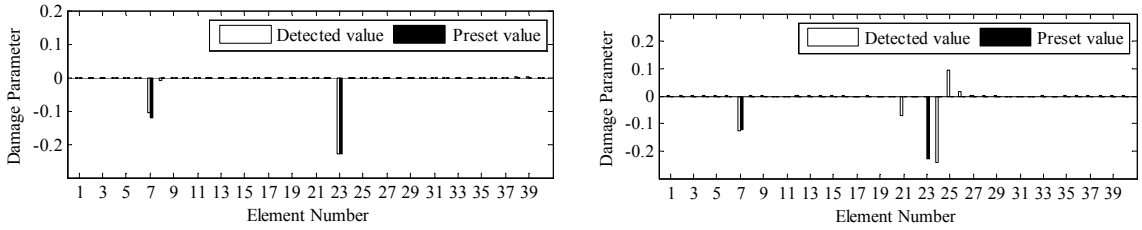


(a) with response reconstruction (b) without response reconstruction

Figure 5.2 Damage identification result

The final damage identification results with response reconstruction are shown in Figure 5.2. For the sake of comparison, the results of damage identification without response reconstruction, namely, only the responses at 11 sensors are used, is also presented in the figure. It can be observed that without response reconstruction, although the damage on element 7 is almost correctly identified, the damage on 23 is falsely located at the adjacent element 24. Besides, there are remarkable positive-errors in element 21 and element 25. The results indicate that the proposed method has certain superiority over the immediate utilization of responses recorded by limited sensors.

## 6. CONCLUSIONS

The multi-scale structural health monitoring (SHM) technologies for large civil structures have been presented in this paper. The accuracy of the proposed technologies has been validated by conducting various experimental studies. The findings from this study advance the existing SHM technologies, allow possible damage detection of large civil structures, and enhance our ability to ensure the functionality and safety of structures.

**AKCNOWLEDGEMENTS**

The authors wish to acknowledge the financial supports from Research Grant Council of Hong Kong (PolyU 5289/12E) and the helps from the PhD students of the first author in preparing this paper.

**REFERENCES**

1. Wang F.Y., Xu Y.L., Qu. W.L. (2014). Mixed-dimensional finite element coupling for structural multi-scale simulation. *Finite Elements in Analysis & Design*, 92, 12–25
2. Zhu S., Zhang X.H., Xu Y.L. and Zhan S. (2013). Multi-type sensor placement for structural health monitoring. *Advances in Structural Engineering*, **16:10**, 1779–1797.
3. Kalman R. E. (1960). A New Approach to Linear Filtering and Prediction Problems, *Transaction of the ASME Journal of Basic Engineering*, **82**, 35-45.
4. Park J., Sandberg I. W. (1991). Universal approximation using radial-basis-function networks. *Neural Computation.* **3: 2**, 246-257.